Geomorphology 402 (2022) 108148

Contents lists available at ScienceDirect

Geomorphology

journal homepage: www.journals.elsevier.com/geomorphology

Multi-proxy characterization of storm deposits on Sanibel Island, Florida: A modern analog for paleotempestology

Joanne Muller [a,*], Christian Ercolani [a], Jennifer Collins [b], Shelby Ellis [c]

[a] Department of Marine and Earth Sciences, Florida Gulf Coast University, 10501 FGCU Blvd S, Fort Myers, FL 33965, USA
[b] School of Geosciences, University of South Florida, 4202 E Fowler Ave, Tampa, FL 33620, USA
[c] Earth and Atmospheric Sciences, Georgia Institute of Technology, North Ave NW, Atlanta, GA 30332, USA

ARTICLE INFO

Keywords:
Hurricane
Storm surge
Overwash
Barrier island
Tempestite

ABSTRACT

Hurricanes have serious impacts on human lives and infrastructure, especially as a result of flooding caused by storm surge and precipitation. To better prepare coastal populations for future hurricanes due to an increasingly warming world, a better understanding of hurricane storm surge is key. Southwest Florida is particularly vulnerable to hurricane storm surge where most of the coastline is within 2.5 m of sea level and population is on the rise (2.5% between 2019 and 2020 in Lee County). This study presents a geologic record of intense hurricane strikes from Sanibel Island dating back to approximately *ca.* 1920. Based on sedimentary proxies such as grain size, organics, moisture content, and calcium carbonate, three tempestites were identified in cores from the Sanibel Island Marsh. Radiometric dating constrained Tempestite 1 as Hurricane Donna (1960) and Tempestites 2 and 3 as the 1926 Great Miami Hurricane and the Tampa Bay hurricane of 1921. Of the eight intense hurricanes (category 3–5) taking place between ~1920–2016, only three hurricanes were recorded in the geologic record. Tempestites 1, 2, and 3 were deposited by intense, large radius storms with significant storm surge, which would indicate that at least three storms made significant impact on the Southwest Florida region between ~1920–1960. Since 1960 no storms have breached the Sanibel Island barrier. It is important for the public to recognize that even though this region has not experienced significant storm surge in the last ~60 years, several hurricanes occurring between 1920 and 1960 produced storms surges greater than ~10 ft. that were able to breach a major barrier island (Sanibel Island). Human-induced climate change is predicted to increase storminess and sea level rise in Southwest Florida with concomitant risk for future storm surge.

1. Introduction

Hurricanes are the single most costly and destructive weather disasters in the United States (Emanuel, 2005). The 2017 hurricane season has been the costliest to date where a series of major hurricanes, including Harvey, Maria, and Irma, were responsible for ~$306.2 billion in damages (NOAA, 2021). In addition to this, the 2020 hurricane season has been the most active to date, with 30 named storms, 14 of which developed into hurricanes, and a record-tying 7 major hurricanes. Of the 30 named storms, 11 of them made landfall in the contiguous United States, breaking the record of nine set in 1916 (NOAA, 2020). Research suggests that a rise in sea surface temperatures, caused by anthropogenic climate change, has led to an increase in the intensity of hurricanes over the last 40 years. This interpretation has, however, been challenged due to the brevity of the historical hurricane record (160 years in the North Atlantic Basin (Landsea et al., 2013)), making it is impossible to assess whether long-term trends in the climate system (centennial to millennial timescales) affect long-term hurricane dynamics. This question can be addressed by means of paleotempestology, a field that utilizes geological proxy techniques to extend the hurricane record (Liu and Fearn, 1993; Liu and Fearn, 2000; Donnelly et al., 2001; Hippensteel, 2011).

Paleotempestology seeks to develop hurricane activities over a large range of timescales, from year-to-year reconstructions to millennial-scale reconstructions. Most long-term paleotempestological records are created using the preserved hurricane overwash signature from storm surge as a hurricane nears the coast. The storm surge will often breach the barrier island and/or dune system, depositing foreshore, offshore and dune sediments into back-barrier lagoons, coastal lakes and/or marshes. Due to close coastal proximity, and their significantly different

* Corresponding author.
E-mail addresses: jmuller@fgcu.edu (J. Muller), cercolani@fgcu.edu (C. Ercolani), collinsjm@usf.edu (J. Collins), saellis@gatech.edu (S. Ellis).

https://doi.org/10.1016/j.geomorph.2022.108148
Received 30 September 2021; Received in revised form 29 January 2022; Accepted 2 February 2022
Available online 7 February 2022

geomorphological and sedimentological depositional characteristics, coastal back-barrier lagoons, bays and marshes are ideal locations for recording high-energy storm surge associated with hurricanes. Hurricane-deposited marine sediments differ from back-barrier lagoon, bay, or marsh sediment in several ways such as: grain size (Donnelly et al., 2001); percent $CaCO_3$ (Leorri et al., 2010); percent organics (Liu and Fearn, 2000) and diatom faunal (Parsons, 1998) and foraminifera composition (Hippensteel and Martin, 1999). The hurricane-deposited signature can vary from site to site, depending on the hurricane's duration and intensity, the site's position relative to the landfall location, the influence of local coastal geomorphology, and the integrity of preservation of the hurricane signature. However, the majority of overwash sediments deposited in back-barrier water bodies form distinguishable layers, often sand or shell, which typically contrast the naturally deposited fine-grained organic-rich or silty background sediment (Liu and Fearn, 2000; Donnelly et al., 2001; Ercolani et al., 2015). By obtaining radiometrically determined age-control points throughout a core, and using the above-mentioned proxies to analyze overwash layers, it is possible to generate much longer hurricane records than the short-term instrumental/historical record.

Paleotempestology has become more contentious in recent years because the exact nature of storm deposition and preservation is somewhat unclear. Some studies find that paleotempestology archives often record more intense events (*e.g.*, Liu and Fearn, 1993, 2000; Donnelly et al., 2001; Donnelly and Woodruff, 2007; Brandon et al., 2013; van Hengstum et al., 2014). Recent work demonstrates that lower category storms, such as those that are larger in size and moving with slower forward speed, can produce significant storm-surge, thereby overwashing barrier islands and depositing storm layers (Hawkes and Horton, 2012; Williams and Denlinger, 2013). There are three primary factors that contribute to the deposition and preservation of paleotempestology archives. First, is related to the storm itself and includes: the site location relative to the hurricane's eyewall; the strength of the storm; the direction of storm movement; and, the overall size of the storm. All of which contribute to the storm surge and therefore the storms' ability to overwash the barrier. Second, the physical characteristics and geomorphology of the lagoonal/marsh barrier and its vulnerability to being breached by storm surge must be considered. Lastly, one must consider the site and its preservational integrity, including: post-depositional erosion; post-depositional lagoonal productivity, including bioturbation and sediment reworking; and lagoonal sediment accumulation rates. Why certain storm events are recorded, and others are not, is generally a combination of the above factors.

The goal of this research was to determine whether historic hurricane events could be identified in a coastal pond on Sanibel Island, Florida. More specifically this research aims to 1) address the sensitivity of the study site to historic hurricane overwash by looking at sediment core sedimentology 2) identify the most useful sedimentary proxies for

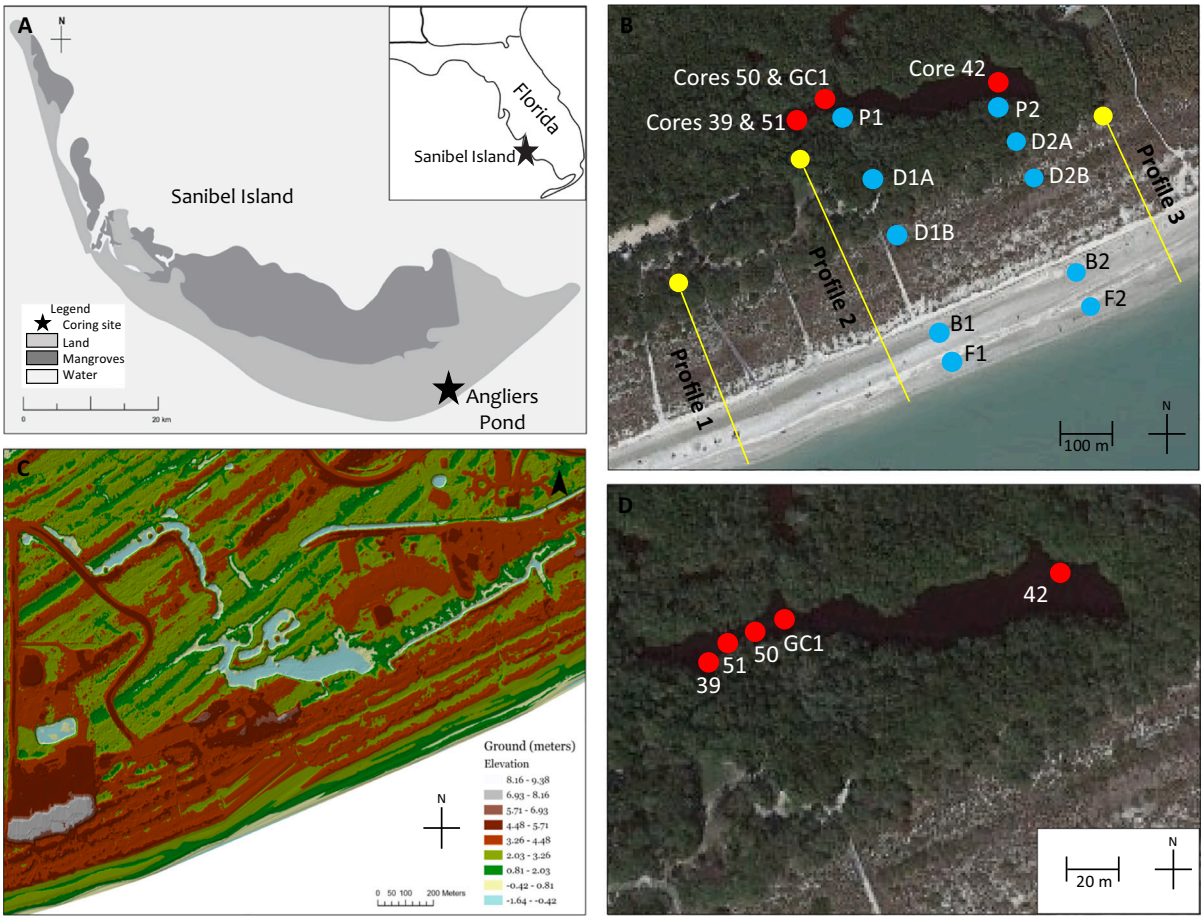

Fig. 1. A) Map of Sanibel Island, including coring site Angliers Pond (black star). Inset shows location of Sanibel, Florida B) Site map showing Angliers Pond with core locations denoted by red circles, sediment sample sources denoted by blue circles and beach profiles denoted by yellow circles and yellow lines C) Digital Elevation Model showing topography of Angliers Pond and the barrier seaward of the pond. DEM created from LiDAR data that were extracted from NOAA Digital Coast archives (https://coast.noaa.gov/dataviewer/#/lidar/search/) and Lee County (https://www.leegov.com/gis/data/lidar-data) D) Angliers Pond highlighting cores locations denoted by red circles: 1305-39 (26.4261941, -82.0646244), 1303-42 (26.4265595, -82.0634055), 1305-50 (26.4262741, -82.0643039) 1410-51 (26.4263263, -82.0644287) and 1610-GC1 (26.4264576, -82.0642149). (For interpretation of the references to color in this figure legend, the reader is referred to the web version of this article.)

measuring hurricane overwash signatures at this site 3) determine the types of storms that overwash into our study site by identifying and naming recent hurricane overwash layers.

2. Study area

2.1. Sanibel Island

Sanibel Island is one of five barrier islands forming the southwestern boundary that encloses the Charlotte Harbor estuarine system (USACE, 1969; Fig. 1A). It is the largest of the five northernmost barrier islands in the complex, and is roughly 19 km long. The island is quite different than others in this region in that it has an arc-shaped hook across its southern end that produces an east–west orientation with a south-facing Gulf shoreline. This orientation reflects a considerably different set of geologic conditions than other barrier islands in this region, exposing coastline that is vulnerable to storm surge of both north-south and east-west oriented hurricanes tracks. This also makes the island ideal for paleotempestology studies.

Sanibel Island contains at least seven distinct sets of beach ridges, with the oldest ridge having a radiocarbon date of 4310 ± 120 years and the youngest being radiocarbon dated at 574 ± 75 years (Missimer, 1973). Initial formation of Sanibel Island likely occurred within 500–800 years of the oldest ridge (Wulfert Ridge). The United States Army Corps of Engineers (USACE, 1969) classifies Sanibel Island as being a null period in terms of growth, except on the northwest shore, where a period of sediment accretion and beach ridge formation has been occurring for the last several hundred years. On the island, longshore currents are the dominant process promoting island migration, and the transgression and regression of the foreshore. The dominant prevailing wind during the winter is northeast, which tends to produce a southward longshore current and sediment transport. During the summer months, the southwest winds are more dominant and produce a northerly sediment transport. However, it is recognized that the winter climatic system is stronger than the summer, resulting in a southerly net longshore transport (USACE, 1969). Seaward of the island, the Florida continental shelf extends out approximately 550 km into the Gulf of Mexico and is composed primarily of carbonate and siliciclastic sediments, with higher percentages of siliciclastic sediments northward of Sanibel Island (Li and Weisberg, 1999).

2.2. Angliers Pond

The Angliers Pond is a brackish back-barrier pond that lies ~125–160 m north of the Gulf of Mexico (Fig. 1A and B). The average salinity of the pond is 5 ppt. The pond is relatively shallow (<0.5 m) and has no present-day tidal connection (Fig. 1C). The pond is surrounded by moderately dense mangroves (~19 trees per 4 m^2) that are mostly *Rhizophora mangle* (red mangrove) with lesser numbers of *Avicennia germinans* (black mangrove). Moving away from the pond *Laguncularia racemose* (white mangrove), *Sabal palmetto* (Sabal Palm) and *Coccoloba uvifer* (Sea Grape) are noted. The canopy density can also be observed in Appendix 1A. The highest elevations between the pond and the Gulf of Mexico (GOM) are associated with the highest dune at ~1.8 m. The terrain slopes down towards the GOM with a series of swales and ridges (Fig. 1C). This is expanded on below in Section 4.1.

2.3. Major hurricanes affecting Sanibel Island, Southwest Florida, from 1870 to 2017

Over the last 135 years, there have been nine major hurricanes (category 3 and above) that passed within 80 km (50 miles) of our field site, causing varying amounts of damage (Table 1 and Fig. 2). We also included the Tampa Bay Hurricane of 1921 in our records due to the significant storm surge reported close to our field site. Unfortunately tide gauge records for this region are not available before 1965 and therefore storms prior to 1965 rely on the historic documentary record. Many of the historic accounts of storm surge used in this study come from locations with varying distances from the study site. For example, the Forts and Barracks at Punta Rassa (8 km) (5 miles), the Caloosahatchee River (~32 km) (~20 miles) Naples (40 km) (25 miles), Marco Island (64 km) (40 miles), and Chokoloskee (97 km) (60 miles). Storms with significant recorded storm surge are outlined below.

In October 1873 a strong Category 3 hurricane made landfall at Punta Rassa, exiting the Florida east coast near Melbourne, Florida. The minimal first-hand accounts indicated that there was considerable loss of life and serious damage to shipping (Ellis, 1984), with the Punta Rassa

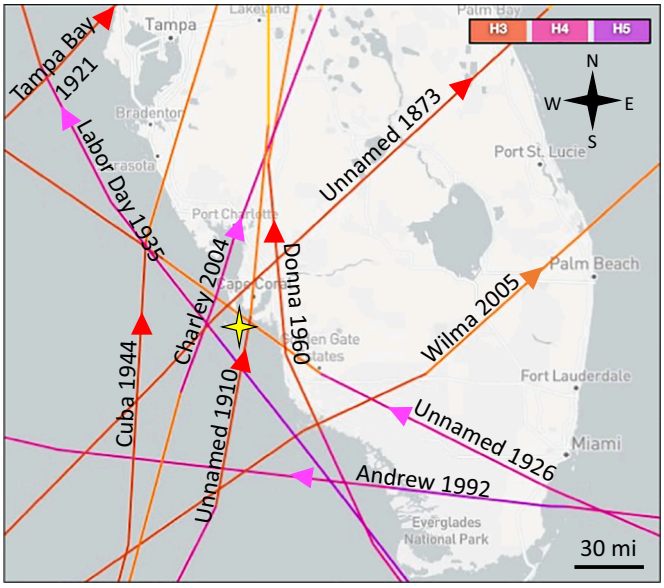

Fig. 2. Sanibel Island Angliers Pond site is denoted by a yellow star. Historic intense hurricane tracks included from NOAA Historical Hurricane Tracks (www.coast.noaa.gov). (For interpretation of the references to color in this figure legend, the reader is referred to the web version of this article.)

Table 1
Southwest Florida hurricane activity between 1870 and 2005.

Year	Name	Category	Storm tide (ft)	Direction	Surge location	Reference
2005	Wilma	3	2.64	SW	Naples Pier	NOAA, 2004
2004	Charley	4	4.36	SSW	Caloosahatchee	Wang et al., 2005
1992	Andrew	4	2.00	E	Ft. Myers Beach	Balfour, 1992
1960	Donna	4	11.00	SSW	Estero Island	Sugg et al., 1971
1944	Cuba	3	11.00	SSW	Naples	Sugg et al., 1971
1935	Labor Day	5	2.00	SSE	Chokoloskee	Coastal Breeze News Staff, 2010b
1926	Great Miami	3	12.00	SE	Punta Rassa	Sugg et al., 1971
1921	Tampa Bay	4	10.00	SSW	Punta Rassa	Sugg et al., 1971
1910	Unnamed	2	10.00	SSW	Marco Island	Sugg et al., 1971
1873	Unnamed	3	14.00	SW	Punta Rassa	Sugg et al., 1971

community completely levelled. Everglades City was flooded with 1.8 m (6 ft) of water (Coastal Breeze News Staff, 2010a). A local Captain noted that Pine Island, approximately 8 km (5 miles) from Sanibel Island, was only saved from storm surge due to the outer barrier islands such as Sanibel (Pine Island Eagle Staff, 2013). The hurricane generated peak winds of 115 mph and a 4.27 m (14 ft) storm surge at Punta Rassa, Florida (Fernández-Partagás and Diaz, 1995; Landsea et al., 2004). The hurricane caused 26 deaths with historical accounts indicating the Schooner *Enterprise* was lost during the storm (Rappaport and Fernández-Partagás, 1996).

In October 1910 an un-named hurricane (known as the Cuba Hurricane or Cyclone of Five Days) made landfall in Southwest Florida as a Category 2 hurricane and caused significant flooding. Storm tide estimates from Marco Island are 3 m (10.0 ft) (Sugg et al., 1971; Landsea et al., 2013). This storm approached SW Florida from western Cuba, with a large radius and slow forward speed before moving along the eastern seaboard of the Carolinas as a tropical storm. The greatest storm surge damage was reported in southern Collier County near Cape Sable and Everglades City (New York Times, 1910), where some accounts recall only escaping inland flooding by climbing trees (Barnes, 2007; Coastal Breeze News Staff, 2010b). In all, it is estimated between Cuba and Florida, at least 101 people died (Barnes, 2007).

The Tampa Bay hurricane of 1921 (also known as the 1921 Tarpon Springs hurricane) was the most recent major hurricane to strike the Tampa Bay Area. Further south Captiva and Sanibel islands were completely inundated with water. In Punta Rassa, the storm tide surge was reported at 3.1 m (10 ft) and the majority of homes were either extensively damaged or washed away. Most highways leading out of Fort Myers were impassable due to high water. Damage to railroad tracks resulted in a suspension of service for three days. On Estero Island, a number of buildings were damaged, including the casinos, cottages, and Crescent Beach resort (The Vicksburg Herald, 1921).

In September 1926 the Great Miami Hurricane caused storm surge damage to Sanibel Island. There are limited reports from this back-door hurricane, exiting the Southwest coast of Florida near Bonita Springs (eastern approach). One indicates a 1.8 m (6 ft) storm surge that caused significant flooded on Sanibel Island, forcing more than half of its residences to relocate. Tide measurements from nearby Punta Rassa indicated storm tides of 3.7 m (12 ft) (Sugg et al., 1971). Furthermore, there are conflicting estimates with associated deaths (243–811 people), financial damages (112–160 million dollars), and citizens made homeless (43,000) associated with the storm (Sugg et al., 1971; Barnes et al., 2007). Wind strength from this storm was the highest ever recorded in U.S. history at the time (123 mph, with some estimates at 150 mph) and the storm decimated the economic boom in South Florida (Barnes, 2007; NOAA, 2021). A recent reanalysis of top damaging hurricanes normalized to the 2018 dollar and societal conditions ranks this storm as the costliest hurricane on record, with estimations at $236 billion dollars if the storm occurred under contemporary societal conditions (Weinkle et al., 2018).

In 1935, the Labor Day Hurricane devastated the Florida Keys and then passed the Southwest Florida coastline as an offshore hurricane. Prior to a recent study by Cerrito et al. (2021) which noted, the Great Havana hurricane of 1946 to be the first record of a Category 5 storm to impact the U.S, this was previously known to be the first recorded Category 5 storm to strike the U.S. (State Library and Archives of Florida, 2017). However, because the hurricane did not make direct landfall in Southwest Florida, maintained a distance of ~40 km (~25 miles) from the coastline, and was very compact (hurricane eye 13-km-wide diameter) (Barnes, 2007; Collins et al., 2017), there were no significant storm surge-related impacts reported in Southwest Florida. One local observed 0.6 m (2 ft) of water inland at Chokoloskee, with other reports of winds at 115 mph in Naples (Coastal Breeze News Staff, 2010b). Further North Tampa Bay saw tides 1.6 m (5.3 ft) above normal. The brunt of the impact was seen further south in the Florida Keys, with storm tidal estimates near Long Key at 3.0–4.5 m (15–20 ft) described by locals as "walls of water" crashing down (McDonald, 1935), with wind estimates between 150 and 250 mph (Sugg et al., 1971; Barnes, 2007). Best estimates for death toll fall around 408–485 victims, caused primarily by the intense hurricane force winds (Barnes, 2007; State Library and Archives of Florida, 2017). Total damage estimates are near $6 million dollars (Barnes, 2007). Because of the serious loss of life tied to the U.S. Army veterans stationed in Lower Matecumbe Key, it propelled the Weather Bureau to establish additional monitoring stations in south Florida to improve disaster preparedness (State Library and Archives of Florida, 2017).

In October 1944 the Cuba-Florida hurricane made landfall near Sarasota, Florida as a Category 2, with the greatest amount of storm surge and beach erosion reported on the beaches near Fort Myers, Florida (Blake et al., 2006). Heavy storm surge was reported in nearby Naples, with tides up to 3.3 m (11.0 ft), while further south the tides near the Everglades were reported at 2.5 m (8.2 ft) (Sugg et al., 1971). Estero Island was inundated by 0.9–1.8 m. (3–6 ft) of water, with 0.9–1.5 m (3–5 ft) of flooding observed on roads upstream of the Caloosahatchee River (Fort Myers News-Press Staff, 1944a, 1944b). While approaching Florida, the storm weakened from a Category 3 (Havana, Cuba at 120–165 mph gusts) to a Category 2. After exiting Florida, this storm hugged the eastern Carolina coast to New England. Overall, it is estimated 18 lives were lost (Sugg et al., 1971). When normalized to 2018 demographics and inflation, this storm would have cost $73.5 billion in damage, making it the seventh most costly hurricane in recent United States history (Weinkle et al., 2018).

In 1960 Hurricane Donna made direct landfall in Naples, Florida as a Category 4 hurricane. Hurricane Donna was responsible for over 11 ft. of storm surge and 12 in of rain in Southwest Florida and approximately $387 to 426 million in damages nationwide at the time (Dunn, 1961; Sugg et al., 1971). Wind gusts up to 115 mph were recorded in Fort Myers, with tides at nearby Estero Island and Naples at 3.0–3.4 m (10–11 ft) and 4 m (10.2 ft), respectively (Dunn et al., 1961; Sugg et al., 1971). In Naples, these tides pushed far inland damaging central city buildings (US Department of Commerce, 1960), with some residents noting at least 3 ft. of water flooding their homes (Marston, 1960). Passing through Florida, Donna maintained hurricane strength as it made additional landfalls in North Carolina (1.2–2.4 m) (4–8 ft. tides) and the New England coast (1.5–3.0 m) (5–10 ft. tides); gusts to 115 mph Long Island, New York) (Sugg et al., 1971). It was noted as "one of the all-time great hurricanes" (NOAA's National Hurricane Center, 1960), claiming 50 lives. Donna is listed as the 5th strongest hurricane to hit the United States and whose name was retired from the hurricane name list and replaced by 'Dora' because of the extreme devastation the storm caused from Puerto Rico north to Canada. If the storm had occurred in 2018, damages are estimated around 50 billion dollars (Weinkle et al., 2018).

3. Methods

3.1. Field work

A theodolite, tripod, and staff were used to obtain a beach profile seaward of the Angliers Pond site to determine the relative vulnerability of the site to storm overwash (Fig. 1B, yellow transect 2). A base elevation on these transects was established using a Trimble RTK unit, model 8A and data was calibrated to NAVD88 datum. LiDAR data was used to compare beach face changes at sites north and south (Fig. 1C, yellow transects 1 and 3 (denoting beach monument markers R-155 and R-156)) of the Angliers Pond. LiDAR data were extracted from NOAA Digital Coast archives (https://coast.noaa.gov/dataviewer/#/lidar/search/). The available data at these monuments is for years 1998, 2004 post Hurricane Charley, 2004 post Hurricane Ivan, 2010, and 2015. Sediment samples were taken from the edge of the pond and along two transects between the pond and the GOM (Fig. 1B, blue markers).

Five cores were taken from Angliers Pond (Fig. 1D) denoted by red

markers: 1305-39 (26.4261941, -82.0646244), 1303-42 (26.4265595, -82.0634055), 1305-50 (26.4262741, -82.0643039) 1410-51 (26.4263263, -82.0644287) and 1610-GC1 (26.4264576, -82.0642149). Cores were taken using a hand-coring technique where a 3-inch diameter aluminum pipe was driven into the sediment using core handles. The sediment compaction within the pipe is then estimated by comparing the sediment height inside the pipe with the remaining portion outside the core pipe. The pipe is then filled with water, capped to provide suction, extracted from the sediment and capped at the bottom. Finally, the excessive pipe length above the sediment-water interface within the pipe is trimmed away, leaving the sediment upper surface flush with the cap.

3.2. Laboratory work

Cores were split, photographed and described at the Florida Gulf Coast University (FGCU) core laboratory. Following this, the cores were sampled at 1 cm resolution, taking special care to avoid contamination between samples. Loss-on-ignition (LOI), moisture content, grain size analysis and calcium carbonate content were used to locate and confirm the presence of tempestites (storm overwash deposits). In addition, ^{210}Pb dating was used to construct age models for the cores used in this study.

Loss-on-ignition determines the percentage of organic content in a sample and distinguishes the inorganic sandy/shelly tempestites from the organic rich back-barrier sediments. Wet samples were placed into pre-weighed aluminum tins and weighed; the samples were dried at 37 °C for 36 h. Once removed from the drying oven, samples were weighted again, and moisture content was calculated. Following the methodology of Dean (1974) and Heiri et al. (2001), samples were placed in a muffle furnace at 550 °C for 5 h after drying. After combustion, the samples were left to cool in the oven; this ensured that samples would not take on atmospheric moisture and that the sample weight was a true ash measurement. All measured weights were recorded, and percentage calculations were performed.

Grain size analysis is a useful proxy in Southwest Florida because tempestites typically contain high concentrations of broken shell material and sand, which can be easily distinguished from the finer-grained background material (Ercolani et al., 2015). To determine percent of coarse-grained sediment, samples were first combusted, then disaggregated, and wet-sieved at 250-μm (modified after Donnelly and Woodruff (2007). Differences in sieve sizes reflect variations in the grain size of suspected paleo-tempestites based on the Wentworth grain size classification scale. The sieves were then placed in a drying oven at 37 °C overnight, and the dry samples were reweighed the following day to determine percent grain size fraction of the sample. Pond background sediment grain size and characterization was performed on core GC1 using a Malvern Mastersizer 3000 particle size analyzer following the methods of Malvern PAnalytical (https://www.malvernpanalytical.com/en/ learn/knowledge-center/user-manuals/MAN0474EN). Sediment samples taken from around the pond, and in transects from the pond to the GOM, were also analyzed for percent organic content using the sample methodology above. These samples were also analyzed for grain size at 63, 250 and 500 μm (Fig. 1B and Appendix 1C).

The calcium carbonate proxy is a useful tool for detecting broken calcium carbonate shell material, carbonate sand, and carbonate mud often found in tempestites. Following the methods of UIC, Inc. (http://www.uicinc.com/carbon-dioxide-coulometer/) samples were placed in a drying oven at 37 °C for 36 h to remove moisture content, then individually homogenized using a mortar and pestle. Samples were then subsampled into approximately 100 mg portions using a microbalance for accuracy. The subsamples were run on a Model CM5014 CO_2 Coulometer. One blank sample and one known standard of 6% calcium carbonate was run before sample trials to ensure the titration cell was working correctly. The coulometric process gives results in basic theoretical units (coulombs) so calibration using standards is not required. Layers rich in shell material appear as spikes in $CaCO_3$% relative to back-barrier sediment deposition.

^{210}Pb isotopic dating was performed on the organic sediment in the upper portions of cores 1305–39 (core 39), 1410–50 (core 50), 1410–51 (core 51). Mainly due to atmospheric deposition, ^{210}Pb is an ideal chronometer for most ecological studies where the ^{210}Pb flux has remained constant over the last 100 years (Appleby and Oldfield, 1978). ^{210}Pb dating involves a U/Th series disequilibrium method where ^{222}Rn escapes from sediments into the atmosphere, where it decays to ^{210}Pb, attaches to aerosols, and finally gets re-deposited (atmospheric fallout) (Appleby and Oldfield, 1978). There are other sources of ^{210}Pb besides atmospheric deposition such as the natural *in situ* production of ^{210}Pb in the soil, called supported ^{210}Pb, which is derived from the existing U and ^{226}Ra (Robbins et al., 1978). This fraction of ^{210}Pb in the soil can be determined by using γ-spectrometry. The difference between the total ^{210}Pb and ^{214}Pb is referred to as the unsupported or excess ^{210}Pb, expressed as $^{210}Pb_{exc}$, which is the atmospheric-deposited amount of excess lead (Pb) and a calculated number that is used for dating (Robbins et al., 1978). The flux of $^{210}Pb_{exc}$ varies throughout the world and is a function of sedimentation rate, where low sedimentation rates yield high $^{210}Pb_{exc}$ values and high sedimentation rates yield low $^{210}Pb_{exc}$ rates (Appleby and Oldfield, 1978).

For the cores dated in this study, samples were removed at 1 cm intervals for the top 10 cms and then more selective sampling was conducted between identified storm events. The intent was to sample downcore to a depth where the $^{210}Pb_{exc}$ concentration is zero. Because lead traces are mostly concentrated in muds and organic-rich sediments, the actual storm layers, which consist mainly of offshore, foreshore, and dune sediments, were excluded from the analysis. Samples were weighed and recorded on a Mettler Toledo balance and placed in a drying oven at 37 °C for 36 h. After re-weighing, samples were sent to MicroAnalytica, Inc. where samples and standards were analyzed using an Ortec Well detector, Model GWL-120230. The sedimentation and sediment accumulation rates were calculated using the CRS (constant rate of supply) model. The CRS model allows sedimentation rates to vary over time and is thus more applicable for shallow SWFL coastal-marine environments where large anthropogenic activities alter the sediment loads (Appleby and Oldfield, 1992; Adhikari et al., 2016). Results from this proxy report the determined depositional year directly above and below each storm event, leaving a "window" of time in which the paleo-tempestite may have been deposited. These windows are then correlated with the known (historical) hurricane record in an effort to name tempestites observed in the geological record.

4. Results

4.1. Beach profiles and sediment samples

During coring efforts in 2016 a beach profile (Profile 2) was taken on the seaward side of the Angliers Pond (Fig. 1B). The beach profile demonstrates a relatively wide foreshore with a series of dune ridges and swales (Fig. 3A). The highest ridge/dune crest is 1.67 m and approximately 45 m from the Gulf of Mexico low tide mark on that day. There is at least 71 m total distance between the pond and Gulf of Mexico (Fig. 3A). If the morphology of the beach has not changed significantly through time it would take a storm surge of at least 1.68 m (~5 ft. and 6 in.) to overwash the 2016 dune ridges.

To assess recent changes to barrier island morphology through time, beach profile data were extracted from the available LIDAR data for Sanibel Island (Fig. 3B and C). At the more northern site, R-155 (Profile 1 Fig. 1B) we note that the dune crest and highest section of the beach is relatively stable through time alternating between ~1.35–1.64 m tall, though the width of the dune crest itself has varied through time. At this site the geomorphology of the foreshore varies significantly (Fig. 3B). The height of the foreshore is lowest in 1998, and also post-Charley and -Ivan in 2004. By 2010 and 2015 the foreshore has gained higher

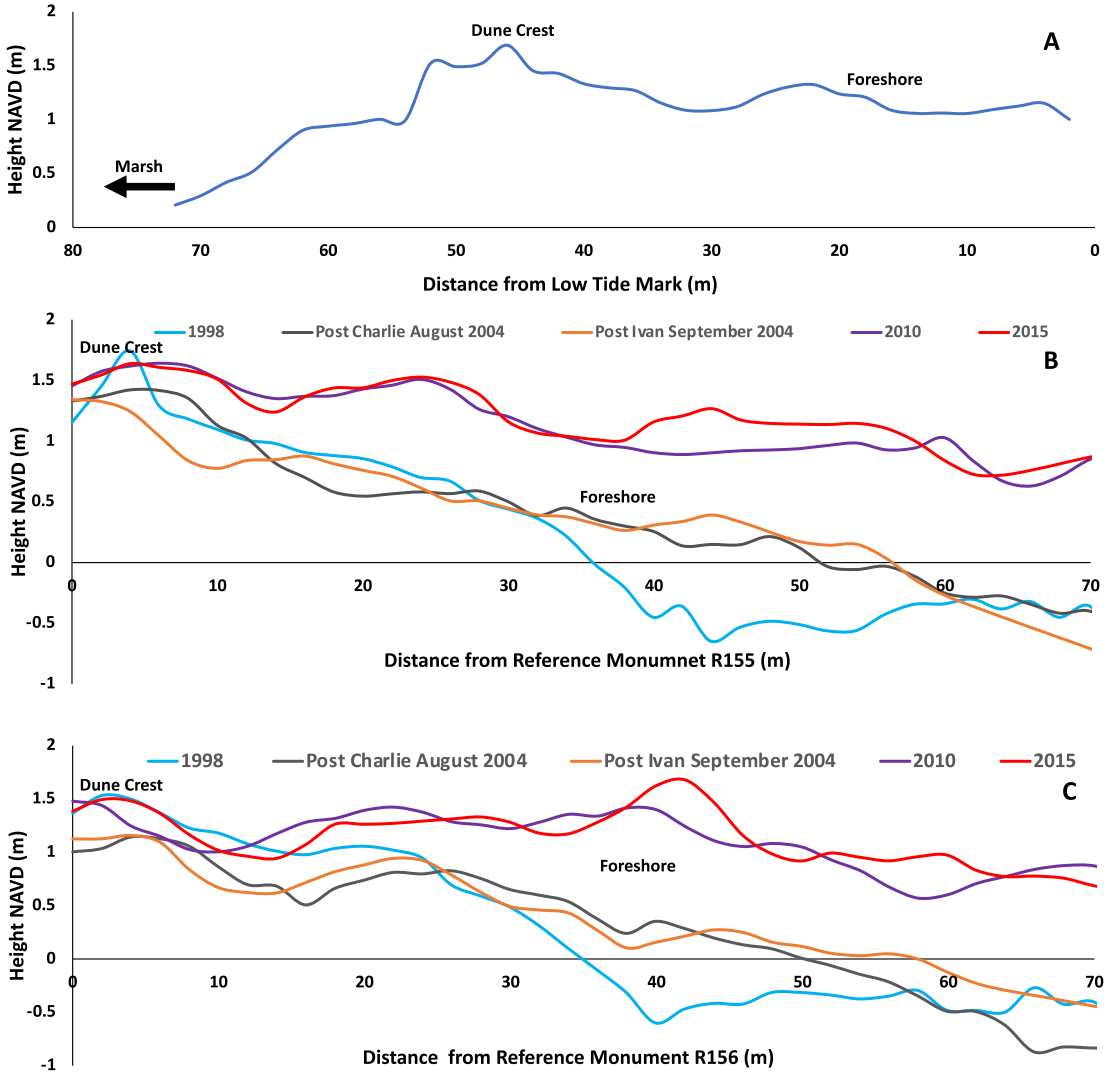

Fig. 3. Beach profiles indicating geomorphology of the barrier island in front (3A) and north (3B) and south (3C) of the Angliers Pond Site. 3A shows the Profile 2 directly in front of the Angliers Pond taken in 2016. Fig. 3B shows beach profile 1 to the north of our site (R-155) and 3C shows beach profile 3 to the south (R-156) of our site for years 1998, 2004, 2010 and 2015.

elevation. At the more southern site, R-156 (Profile 3 Fig. 1B), we note that like R-155 the dune crest and highest section of the beach is relatively stable through time alternating between ~1.15–1.5 m tall, at this location the width of the dune crest itself hasn't varied significantly through time. Similar to R-155 this site sees significant foreshore variability through time (Fig. 3C). Just like R-155 the height of the foreshore is lowest in 1998, and also post-Charley and -Ivan in 2004. By 2010 and 2015 the foreshore has gained higher elevation.

Sediment samples taken around the pond and between the pond and GOM are reported on in Appendix 1C. Samples Pond 1A and 2A, taken from the pond's edge, consist of ~20 and 32% organic content, 2 and 6% clay and silt, 75 and 60% very fine-fine sand, 3.6 and 2.65% medium sand and 1 and 0.6% coarse sand. Samples Pond 1B and 2B were take 1 m away from samples Pond 1A and 2A moving away from the pond. These samples consist of ~3 and 31% organic content, 5.5 and 7% clay and silt, 81 and 67% very fine-fine sand, 9 and 12% medium sand and 1 and 1% coarse sand. Samples Pond 1C and 2C were take 1 m away from samples Pond 1B and 2B moving away from the pond. These samples consist of ~13 and 5% organic content, 11.2 and 8.7% clay and silt, 66.1 and 72.3% very fine-fine sand, 6.6 and 10.2% medium sand and 0.6 and 3.1% coarse sand. Two dune samples were taken in each transect (Dune 1A, 1B, 2A and 2 B). All dune samples have high percentages of very fine and fine sands ranging from 65 to 86%, with lesser amounts of medium sands ranging from 3 to 18%. Berm and foreshore sediment were more poorly sorted. Berm samples have high percentages of fine (49–50%) and medium sands (33–40%), with lesser amounts of coarse sand (7–14%). The foreshore sediments also have high percentages of fine (46–50%) and medium sands (30–35%), with the highest coarse sand content (12–22.5%).

4.2. Radiometric dating

$^{210}Pb_{exc}$ was used to provide age assessment in the uppermost sediment samples of cores 39, 50, and 51 from Sanibel Island (Fig. 4, Appendix 1B). In cores 39 and 51, cesium isotope 137 (^{137}Cs) was also measured. Table 1 also shows the associated errors with the $^{210}Pb_{ex}$, CRS age measurements and the ^{137}Cs concentrations. Age points between measurements were interpolated by calculating sedimentation rates throughout the core.

In core 50, twelve sediment samples were analyzed for $^{210}Pb_{ex}$ and ^{137}Cs content (Fig. 4, Appendix 1B). The core shows low $^{210}Pb_{ex}$ concentrations in the top sample (0–1) but then high $^{210}Pb_{ex}$ to low $^{210}Pb_{ex}$ is seen between 2 and 55 cm. The $^{210}Pb_{exc}$ decay profile for this core has an R^2 value of 0.92. Unfortunately, the ^{137}Cs concentrations in this core

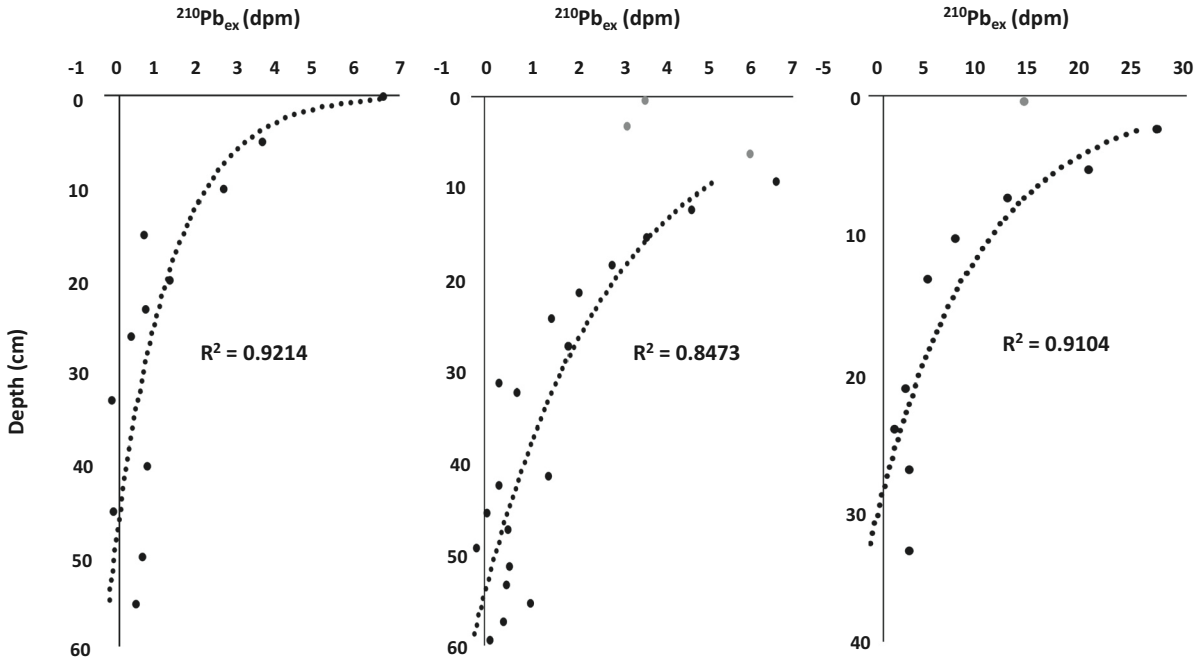

Fig. 4. Downcore $^{210}Pb_{ex}$ decay profiles for cores 1305-39, 1410-50, 1410-51.

were all below the detection limit, except the core top (0–1 cm) (Fig. 4, Appendix 1B). In core 51, twenty-two sediment samples were analyzed for $^{210}Pb_{ex}$ and ^{137}Cs content (Fig. 4, Appendix 1B). This core also shows low $^{210}Pb_{ex}$ concentrations in the two top samples (0–1 and 3–4 cm) but then high $^{210}Pb_{ex}$ to low $^{210}Pb_{ex}$ is seen between 6.5 and 60 cm. The $^{210}Pb_{ex}$ decay profile for this core has an R^2 value of 0.84. The ^{137}Cs concentrations in this core were highest at 3.5, 9.5 and 24.5 cm (Fig. 4, Appendix 1B). In core 39, ten sediment samples were analyzed for $^{210}Pb_{ex}$ and ^{137}Cs content (Fig. 4, Appendix 1B). This core also shows low $^{210}Pb_{ex}$ concentrations in the top sample (0–1) but then high $^{210}Pb_{exc}$ to low ^{210}Pb is seen between 2 and 34 cm. The decay profile for this core has an R^2 value of 0.91. Like core 50, core 39 has very low to below detection limit ^{137}Cs concentrations.

The average sedimentation rates for cores 39, 50, and 51 are 0.87, 0.41 0.65 cm yr^{-1}, respectively (Appendix 1B) which yields an overall pond average of 0.64 cm yr^{-1}. These values exclude the highlighted sections, which are assumed to be the products of overwash events rather than normal deposition. Overwash events do not represent typical pond sedimentation since most of the sediment deposition is related to one storm surge event.

4.3. Core sedimentary proxies

The Angliers Pond cores used to interpret the paleotempestological record include, 1305–39 (39), 1303–42 (42), 1305–50 (50), 1410–51 (51) and 1610-GC1 (GC1). Pictures for cores 39, 42, 50, 51 and GC1 are provided in Fig. 5. All core pictures show a general transition from quartz dominated fine to medium grained sands in the core bottoms to finer grained, organic rich, muds in core tops (Fig. 5). These sediment transitions are noted at 30, 40, 45, 48 and 58.5 cm in cores 39, 42, 50, 51 and GC1 respectively. Cores taken closer to the edge of the pond, contain a higher percentage of organic material in the core tops than compared to those taken closer to the center of the pond.

Stratigraphic logs, moisture content, LOI and percent grain-size, and percent calcium carbonate proxies were used to delineate more clearly the down-core tempesites (Figs. 6 & 7). Core 39 is 93 cm in length and

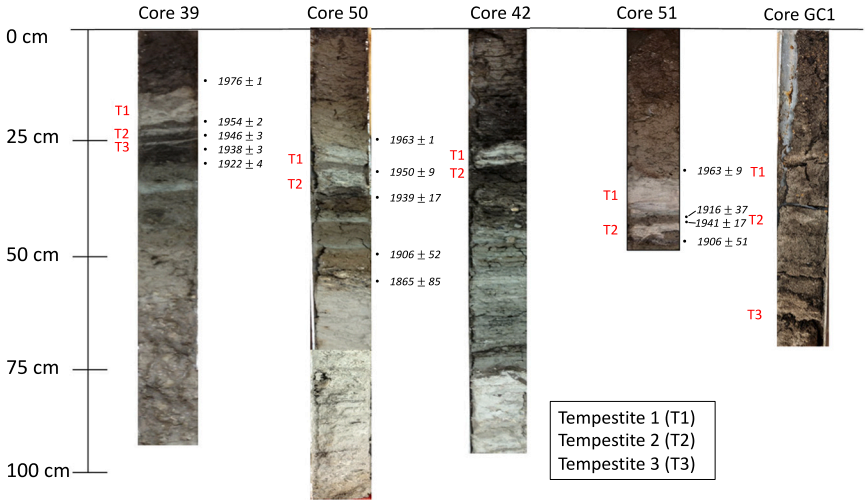

Figure 5. Core photographs for cores 1305-39, 1303-42, 1305–50, 1410–51 and 1610-GC1.

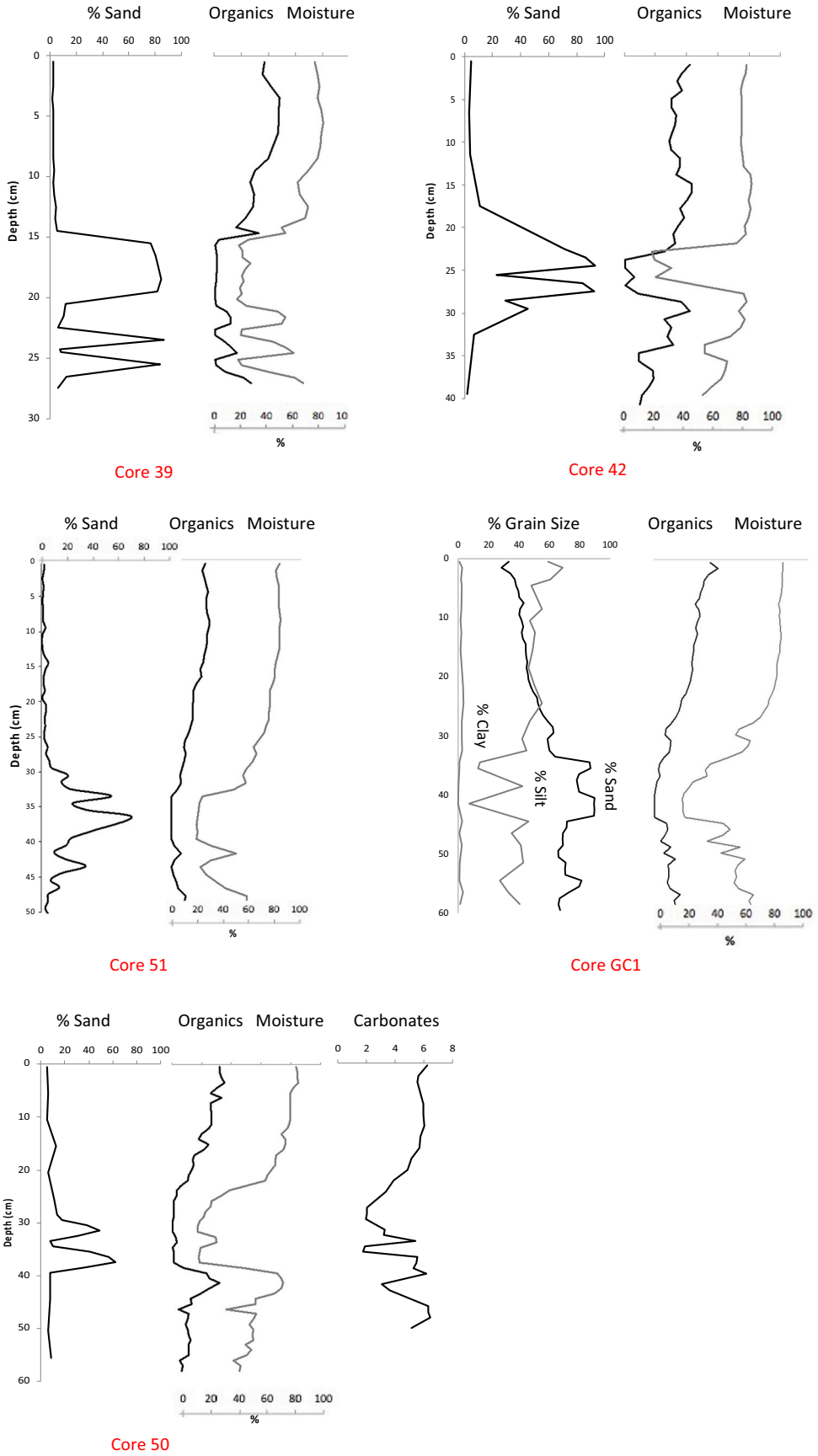

Fig. 6. Sediment proxies for cores 1305-39, 1303-42, 1305-50, 1410-51 and 1610-GC1. Sand grain size (>250 μm) low moisture content, and high inorganic content are indicative of the tempestite layers in all cores.

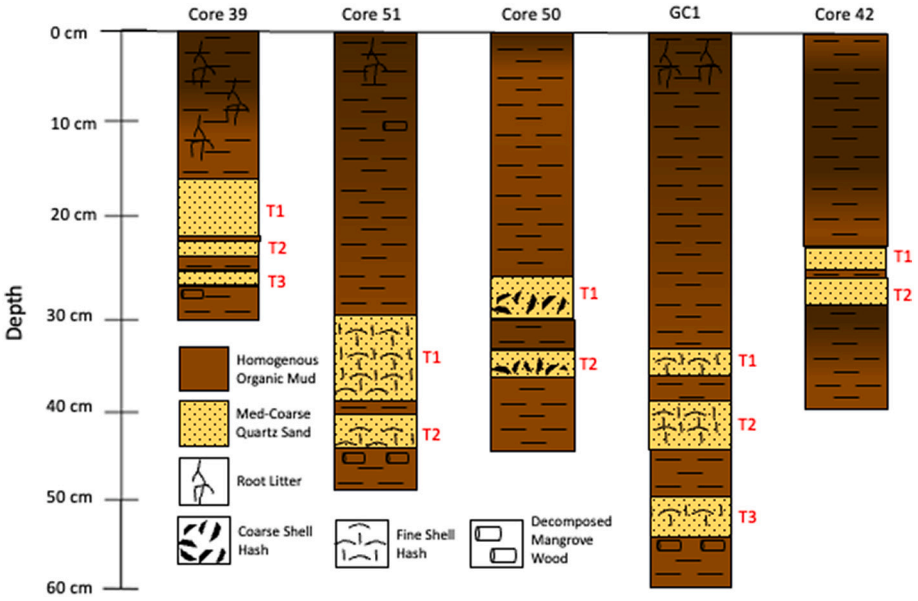

Fig. 7. Stratigraphic columns for cores 1305-39, 1303-42, 1305-50, 1410-51 and 1610-GC1

displays three possible tempestites (T1, T2, T3) that occur between 15 and 21 cm, 22–23 cm, and 25–26 cm, respectively (Fig. 6). Low organic and moisture content correspond to the high concentrations of quartz sand at these depths. All three layers are composed primarily of poorly sorted, medium-coarse grained quartz sands with no evidence of sedimentary structures that are sometimes noted in other paleotempestology studies (Myrow and Southard, 1996). The background sediments between 0 and 30 cm consist of a fine-grained organic mud. Sediments below 30 cm consist of carbonate and quartz sands. The color of the mud is darkest brown in the core top, corresponding to highest organic content. Root litter is noted in the top 15 cm of core 39 (Fig. 7).

Core 51 is 59 cm in length and contains two possible tempestites (T1, T2) consisting of quartz sand and fine shell hash occurring at 33–40 cm and 42–44 cm, respectively (Fig. 6). These layers are primarily composed of poorly sorted fine-coarse grained quartz sand with fine shell hash present in both T1 and T2. No evidence of sedimentary structures are noted in T1 and T2. Grain-size analyses confirms the presence of one thick (T1) and one thin tempestites (T2). The percent organic analysis shows a rapid increase in inorganic content around 33–39 cm (T1) and 42–43 cm (T2). The tempestites are embedded among organic mud background sediment. Low organic and moisture content correspond with T1 and T2. The background sediments between 0 and 48 cm consist of organic muds. The color of these muds gets progressively darker in brown color towards the core top, corresponding to highest organic content. Some root litter is present in the top 5 cm of the core and decomposed wood is also present at depths of 11 cm and again at 45 cm. Sediments below 48 cm consist of carbonate and quartz sands (Fig. 7).

Core 50 is 124.5 cm in length and displays two possible tempestites (T1, T2) consisting of poorly sorted, fine-coarse grained quartz sand and coarse shell hash. The shell hash is mostly present towards the bottom of both T1 and T2, indicating a fining upwards sequence. No other sedimentary structures are noted. Low organic and moisture content correspond to the high concentrations of sand and coarser grain sizes corresponding with T1 and T2. Separated by another sandy mud lamination, T2 spans from 33 to 37 cm and is composed of a coarse-grained quartz sand matrix mixed with coarse shell hash. Grain size and calcium carbonate analyses confirm two distinct peaks in both grain size and calcium carbonate that correspond to T1 and T2 (Fig. 6). The tempestite layers are embedded in organic mud between 0 and 45 cm. No structures are noted in the background sediment; however, the mud is slightly darker brown in color in the top 5 cm, corresponding to highest organic content. Sediments below 45 cm consist of carbonate and quartz sands (Fig. 7).

Core GC1 is 70 cm in length and contains three possible tempestites (T1, T2 and T3) consisting of quartz sand and fine shell hash that occur at 56.5–50.5 cm, 44.5–39.5 cm and 36.5–33.5 cm respectively (Fig. 6). The layers are primarily composed of poorly sorted medium-coarse grained sands with no evidence of sedimentary structures. Low organic and moisture content correspond with T1, T2 and T3. Percent grain-size is also high within T1, T2, and T3. The tempestites are embedded among organic muds (50–60% silt and $<$ 5% clay concentrations). No structures are noted in the background sediment; however, the mud is slightly darker brown in color in the top 10 cm, corresponding to highest organic content. Root litter is also present in the core top (0–8 cm). Sediments below 58.5 cm consist of carbonate and quartz sands (Fig. 7).

Core 42 is 126 cm in length and contains two possible tempestites (T1, T2). Tempestites consist of poorly sorted, fine-coarse grained quartz sands at 24–26 cm and 27–28 cm, respectively with no evidence of sedimentary structures (Fig. 6). Low organic and moisture content correspond with T1 and T2. The organics-proxy (LOI) does not show clear delineation between T1 and T2 because the thin lamination between the sand beds also contains high amounts of silt making differentiation difficult. The background sediments between 0 and 40 cm consist of organic muds. Darkest brown muds exist at 15–33 cm, corresponding to highest organics. Sediments below 40 cm consist of carbonate and quartz sands (Fig. 7).

4.4. Age ranges of tempestites

In core 39, the LOI, moisture, and grain size analyses (Fig. 6) indicate the presence of three paleo-tempestites at (T1) 15-21 cm; (T2) 22–23 cm; (T3) 26–27 cm. Using the ^{210}Pb and CRS model the age range for paleo-tempestite 1 (T1) has been approximated between at *ca.* 1961 ± 5 YR and *ca.* 1984 ± 1 YR by the lower and upper sediments in which the paleo-tempestite is embedded. Paleo-tempestite 2 (T2) has been approximated between at *ca.* 1951 ± 10 YR and *ca.* 1961 ± 5 YR by the lower and upper sediments in which the paleo-tempestite is embedded. Paleo-tempestite 3 (T1) has been approximated between at *ca.* 1938 ± 20 YR and *ca.* 1951 ± 10 YR by the lower and upper sediments in which the paleo-tempestite is embedded (Table 2).

Table 2
Age ranges of Tempestites 1, 2, and 3 based on ^{210}Pb dating and CRS models.

Core number	Depths (cm)	Time ranges (yrs.)	Time ranges including error
Tempestite 1			
39	21.5–13.5	1961 ± 5–1984 ± 1	1956–1985
50	33.5–26.5	1950 ± 9–1956 ± 3	1941–1959
51	41.5–32.5	1957 ± 11–1963 ± 9	1946–1972
Average		1956 ± 8–1967 ± 4	1948–1971
Tempestite 2			
39	24.5–21.5	1951 ± 10–1961 ± 5	1941–1966
50	40.5–33.5	1939 ± 17–1950 ± 9	1922–1959
51	42.5–41.5	1916 ± 37–1941 ± 17	1879–1958
Average		1935 ± 21–1950 ± 10	1914–1960
Tempestite 3			
39	27.5–21.5	1938 ± 20–1951 ± 10	1918–1961

In core 50, the LOI, moisture, grain size and calcium carbonate analyses (Fig. 6) indicate the presence of two paleo-tempestites at (T1) 29–33 cm and (T2) 34–39 cm. Using the ^{210}Pb and CRS model the age range for paleo-tempestite 1 (T1) has been approximated between at *ca.* 1950 ± 9 YR and *ca.* 1956 ± 3 YR by the lower and upper sediments in which the paleo-tempestite is embedded. Paleo-tempestite 2 (T2) has been approximated between at *ca.* 1939 ± 17 YR and *ca.* 1950 ± 9 YR by the lower and upper sediments in which the paleo-tempestite is embedded (Table 2).

In core 51, the LOI, moisture, and grain size analyses (Fig. 6) indicate the presence of two paleo-tempestites at (T1) 33–39 cm and (T2) 42–46 cm. Using the ^{210}Pb and CRS model the age range for paleo-tempestite 1 (T1) has been approximated between at *ca.* 1957 ± 11 YR and *ca.* 1963 ± 9 YR by the lower and upper sediments in which the paleo-tempestite is embedded. Paleo-tempestite 2 (T2) has been approximated between at *ca.* 1916 ± 37 YR and *ca.* 1941 ± 17 YR by the lower and upper sediments in which the paleo-tempestite is embedded (Table 2).

5. Discussion

5.1. Age model

^{210}Pb sediment dating in the Southwest Florida region can sometimes present challenges. Radionuclides, such as ^{210}Pb, adsorb more readily to organic-rich fine-grained particles with higher surface areas, leading to higher accumulation rates in sediments that have higher percentages of fine-grained particles (Singleton et al., 2017). Fortunately, the Angliers Pond has relatively high concentrations of organics and fine-grained sediments and therefore the ^{210}Pb activities tended to be relatively high (Fig. 4) in comparison to other Southwest Florida coastal sites (Savarese et al., 2006). In all cores we tend to see low ^{210}Pb activities in core tops (~0–2 cm). This may indicate that the very top sediments are disturbed. However, below these samples, in all cores, the decay is relatively constant through time with R^2 values of 0.92, 0.85 and 0.91 for cores 1305–50, 1410–51 and 1301–39 respectively (Fig. 4).

5.2. Evolution of the Angliers Pond

A clear transition is noted in all cores where the sediments indicate a change from a high-energy marine setting (fine-medium grained quartz and carbonate sands) to a low-energy setting (organics and silts with lesser amounts of fine quartz sand). This transition is marked at 30, 40, 45, 48 and 58.5 cms in cores 39, 42, 50, 51 and GC1 respectively (Fig. 5). Research from Missimer (1973) has identified that the Angliers Pond is presently located on a strand plain, (identified as stand plain (beach ridge plain) number 7 in Missimer, 1973). Sanibel Island is home to multiple strand plains where well-defined parallel, or semi-parallel, sand ridges separated by shallow swales can be observed. The swales between these sand ridges are long, narrow, generally shallow, trough like, elongated depressions. They are aligned roughly parallel with the coastline (Missimer, 1973; Otvos, 2000).

It is likely that Anglier Pond is an inter-swale pond, sometimes referred to as a cat's eye pond. These ponds can form along coastlines that have prograded seaward leaving a field of secondary dune ridges. The secondary dune ridges and intradune swales are quickly colonized by plants. As the landscape and plant succession matures, two processes can occur that contribute to pond formation. After many years of precipitation and evaporation, the older landscapes on the backshore develop shallow groundwater lenses. The water table tends to be closer to swale surfaces than the surfaces of the dune ridges and during wet seasons the water table may actually intercept the swale surface creating ponds. The secondary process effecting swale pond development is the succession of vegetation on the swale surface. After many years the density of plants in a swale becomes high leaving the swale surface enriched with living and dead organic material. The organic material is less permeable than the original sand and therefore, rainwater percolates into the groundwater at much slower rates. Surface water can eventually get perched above the swale surface forming ponds (Oertel, 2005).

This is in line with the elongated shape of the Angliers Pond and its parallel orientation with the coastline. In addition, Angliers Pond has well-developed vegetation around its periphery (Appendix 1A, vegetation DEM) and brackish water at 5 ppt. The low brackish salinities may be due to tidal wicking from the water table at the site. Sediment samples from the pond edge indicate organic concentrations of 18–30%, with high concentrations of silt-fine sand (64–77%). More importantly this characterization is also in line with the recent work of Savarese et al. (2019) that show recent progradation of the coastline seaward of Angliers Pond. This research shows the progradation of the foredune crest seaward between 1995 and 2016 (Appendix 1D, Fig. 104).

The pond background sediments mark the beginning of the true modern storm record where overwash sediments are clearly delineated from background sediments. Overwash sediments are also different to the sediments taken at the ponds edge (Fig. 2B, P1&P2) that mostly consist of organics, silts and very-fine sand. The sediments that are most similar to the overwash sediments in Angliers Pond are the samples taken from the foreshore seaward of Angliers Pond (Fig. 1B). These sediments are poorly sorted with fine-coarse quartz sands and broken shell.

It is possible that below the pond sediments, within the swale/open bay sediments, older overwash events exist. This can be seen in the core photographs, in particular cores 39, 42 and 50 (Fig. 5) where lighter sediments layers (usually 2 in each core) are delineated against slightly darker background sediments. However, it is difficult to constrain these potential tempestites because in these core sections the background sediment is mostly inorganic, fine-medium grained sands. For this reason, we did not sample further down into our cores. But the presence of these layers in the core pictures do give us encouraging information that perhaps other field sites on Sanibel Island may allow us to extend the paleotempestology record further back in time. Several intense hurricanes made landfall before the inception of the pond sediments, such as the 1873 and 1910 storms which have reported storms surges at Punta Rassa of 14 and 10 ft. in the region (Table 1; Sugg et al., 1971). It is expected that these surges would have overwashed the barrier. But unfortunately, our site is not ideal for preserving these particular events because the pond itself is not old enough.

5.3. Tempestite identification and correlation with historic storms

Cores 42, 50, and 51 exhibit similar stratigraphy (Figs. 6 & 7) displaying only two tempestites, whose positioning in the cores show strong correlation; while cores 39 and GC1 exhibit similar stratigraphy

(Figs. 6 & 7) displaying three tempestites. Table 2 shows all of the date ranges for T1, T2, and T3 from ^{210}Pb dated cores. Because these events have occurred in the last 100 years, tempestites should correlate to the documented historical hurricane record.

Tempestite 1 in cores 39, 50, and 51 has the following age ranges:1961 ± 5 to 1984 ± 1, 1950 ± 9 to 1956 ± 3 and 1957 ± 11–1963 ± 9 (Table 2). These age ranges, including errors, are 1956–1985, 1941–1959 and 1946–1972. Average age ranges are 1956 ± 8 to 1967 ± 4. For the time period associated with T1, the only major hurricane that made landfall near Sanibel Island, and produced a significant storm surge capable of back-barrier beach sediment deposition, was Hurricane Donna in 1960 (Category 4). Unfortunately, Hurricane Donna made landfall before tide gauges were installed in 1965 and therefore storm surge values are sourced from the historic record. These storm surge estimates from the historic record are reported at 3.34 m (11 ft) at Estero Island, approximately 16 km (10 miles) south of the Angliers Pond site. Due to the present-day height of the barrier seaward of the Angliers Pond site, which is 1.67 m tall (5.8 ft), overwash with a 3.34 m (11 ft) storm surge would be highly likely.

Further downcore T2 and T3 are more difficult to constrain due to the greater error associated with the ^{210}Pb dating (Table 2). The larger error estimation associated with T2 and T3 is a product of the Binford model used to calculate the ages. Based on a 95% confidence interval, the accuracy of a specific date decreases with depth, as Pb concentrations also decrease (Binford, 1990). Therefore, dates further down the core, where the concentration of Pb is less, have more variability and are less reliable than those occurring closer to the surface.

Nonetheless, T2 in cores 39, 50, and 51 have the following age ranges: 1951 ± 10 to 1961 ± 5, 1939 ± 17 to 1950 ± 9 and 1916 ± 37 to 1941 ± 17 (Table 2). These age ranges, including errors, are 1941–1966, 1922–1959, and 1879–1958. Average age ranges are 1935 ± 21 to 1950 ± 10. Tempestite 3 is only seen in two cores and only one of these cores, core 39, was dated with ^{210}Pb. The time range is 1938 ± 20–1951 ± 10 and the age range, including error, is 1918–1961. What is clear from the ^{210}Pb dating is that the intervals for T2 and T3 are very long-time spans and they are similar for both T2 and T3. This may simply be due to the large ^{210}Pb dating errors in the deeper samples, but we believe the more likely explanation is that in many of our cores, such as 50, 42, and 51, T2 is actually two storm overwash events that occurred relatively close together in time. In other words, that T2 in some of our cores is T2 and T3 combined, without the background sedimentation existing between these two tempestites.

The early 1900's was an active time period for Southwest Florida during which several intense hurricanes made landfall in the region. During the T2 and T3 intervals, suggested by the ^{210}Pb dating, there are four possible hurricane landfalls that likely affected Sanibel Island: The 1944 Florida-Cuba Hurricane, the 1935 Labor Day Hurricane, the 1926 Great Miami Hurricane, and the 1921 Tampa Bay Hurricane. Because overwash deposition is mostly an artifact of storm surge, and tidal gauges were absent from the region up until 1965, we are forced to rely on the historic storm surge records of these hurricanes.

Historic storm surge estimates for the 1944 Florida-Cuba Hurricane are not available for Sanibel Island, or the close-by Punta Rassa barracks/wharf, and therefore the extent of the storm surge is largely unknown for our field site. A storm surge of 3.35 m (11 ft) was reported in Naples, however closer to Sanibel Island 1.5–1.8 m (5–6 ft) of flooding was observed on roads upstream of the Caloosahatchee River. The Florida-Cuba Hurricane was a Caribbean forming storm, passing directly over the western end of Cuba as a Category 4 storm, however after passing over Cuba it weakened to a Category 3 storm as it approached Florida. As it passed Naples it further weakened to a Category 2 storm, with winds about 90 kts as it passed by Sanibel Island. In this case, the upper right-hand quadrant would have been over the water and therefore may have produced significant storm surge. However, due to the weakening of the storm as it travelled north, it is likely that the surge may not have been as significant on Sanibel Island as that recorded in Naples. If the storm surge at Sanibel Island was comparable to Naples it would likely overwash the barrier between our site and the Gulf of Mexico. However, if the surge was more like the 5–6 ft. reported in Fort Myers along the Caloosahatchee River this storm surge would be unlikely to breach the barrier in front of our field site on Sanibel Island. For this reason, we do not believe that T2 or T3 represent the 1944 Florida-Cuba Hurricane.

Historic storm surge estimates are even more difficult to locate for the 1935 Labor Day Hurricane. At the time, this was the first recorded Category 5 storm to strike the United States. This was a Cape Verde hurricane and made landfall as a Category 5 in the Florida Keys with a recorded storm surge of 5.5 to 6.1 m (18 to 20 ft). The storm then moved northwest hugging the Southwest Florida coastline and weakened to a Category 4 storm as it travelled past Naples and then Sanibel Island. The historic track may indicate that the eyewall was over land for some of this time period, which may have decreased the storm surge in the Southwest Florida region. Closest historic storm surge estimates of 0.6 m (2 ft) come from Chokoloskee, south of Naples, Fl. A 2 ft. storm surge would not have produced overwash deposition on Sanibel Island. For this reason, we do not believe that T2 or T3 represent the 1935 Labor Day storm.

There are limited reports on the 1926 hurricane, which was a Category 4 back-door hurricane, exiting the Southwest Florida coast near Bonita Springs as a Category 2 storm (eastern approach). Some historic reports indicate a peak storm tide of 3.4 to 3.7 m (11 to 12 ft) at Punta Rassa and the islands of Captiva and Sanibel, completely flooding Sanibel Island with salt water (Sugg et al., 1971; Doyle et al., 1984; Edic, 1996). The surge on Sanibel however was reported as a 6 ft. storm surge (Pielke and Landsea, 1998). The storm was said to have opened Redfish Pass between Captiva and North Captiva islands (Edic, 1996). Assuming a similar barrier height of 5 ft. between, it is highly likely that this storm would have overwashed marine sediment into the Angliers Pond, especially if it had a storm-tidal surge of 3.5 m (11–12 ft).

The Tampa Bay hurricane of 1921 formed in the Caribbean and strengthened further in the Gulf of Mexico to a Category 4 storm. The storm was quite far offshore as it passed Captiva and Sanibel islands (~193 km) (~120 miles). However, historic reports indicate that the islands were completely inundated with water. In Punta Rassa, a storm surge of 3.05 m (10 ft) was reported along with most homes being either extensively damaged or washed away. Most highways leading out of Fort Myers were impassable due to high water. Damage to railroad tracks resulted in a suspension of service for three days. On Estero Island, a number of buildings were damaged, including the casinos, cottages, and Crescent Beach resort (The Vicksburg Herald, 1921).

In summary, the dating and proxy results for cores 39 and 50 indicate that T1 was formed by Hurricane Donna (1960). The storms that produced T2 and T3 are more difficult to discern due to the greater ^{210}Pb ranges and dating errors. However, the historic records discussed above would indicate that T2 and T3 were most likely produced by the 1926 Great Miami Hurricane and the Tampa Bay hurricane of 1921. The 1926 Great Miami Hurricane and the Tampa Bay hurricane of 1921 may also make the most sense, due to the lack of background deposition found between T2 and T3. We hope that future studies in the region, on higher sediment accumulation rate cores, may help in answering these questions.

5.4. Sensitivity of Angliers Pond to hurricane overwash and subsequent deposition

This research found evidence of historic hurricane overwash events in the sediments of Angliers Pond on Sanibel Island, Florida. The first goal of the study was to address the sensitivity of the study site to historic hurricane overwash by looking at sediment core sedimentology. We found evidence of three overwash events in the Angliers Pond sediment cores between ~1920–2017. Not every core displayed evidence of three clear tempestites, which we may be due to the brevity

between two historic storms (1926 Great Miami Hurricane and the Tampa Bay hurricane of 1921). In this case two tempestites may look like one tempestite due to the lack of significant sedimentation between events. This has been found in other studies for example Hurricanes Gustav and Ike made landfall only 2 weeks apart from one another in 2008, therefore appearing as one event horizon (Dietz et al., 2021). In addition, Williams and Liu (2021) found that the tempestites deposited by Hurricanes Carla (1961) and Audrey (1957) where difficult to distinguish from one another using sedimentology and stratigraphy alone. This time period of four years between storms is more consistent with what we might be seeing in Angliers Pond where the 1926 Great Miami Hurricane and the Tampa Bay hurricane of 1921 (five years apart) may have occurred too close together in time to see significant background sedimentation between events.

Another goal of this research was to determine the most useful sedimentary proxies for measuring hurricane overwash signatures on Sanibel Island. We found grain-size to be the most useful proxy in differentiating between background pond sediments (predominantly silts and organics with some fine sand) and the storm overwash layers (predominantly medium-coarse grained quartz sands with calcium carbonate shell hash). The LOI proxy was also useful, but due to the high concentrations of silt (50–60% in GC1) in background sediments tempestites are not always clearly defined using this proxy alone. In addition, we found the calcium carbonate proxy to be helpful in differentiating overwash layers when shell hash was present. As shown in this study and many other paleotempestology studies a multi-proxy approach tends to be best practice (*e.g.*, Liu and Fearn, 2000; Donnelly et al., 2001; Leorri et al., 2014; Ercolani et al., 2015).

Lastly, we wanted to gain an understanding of the types of storms that overwash into our study site by identifying and naming recent hurricane overwash layers. What is evident from the Angliers Pond upper-most sediments is that not all hurricanes coming within 80 km (50 miles) of Sanibel Island are being archived in the sedimentary record. Of the eight hurricanes listed as category 3–5 (Table 2) making landfall between ~1920–2016 (approximate age of the Angliers Pond) only 2–3 storms are represented as paleotempestites. Interestingly, the ^{210}Pb dating indicates that these modern paleotempestites (T1, T2, T3) are deposited by significant storm surges, produced by category 3–5 hurricanes. Indicating that Angliers Pond is more sensitive to intense hurricanes, with significant storm surge rather than all historic hurricanes tracking within 50 miles of Sanibel Island. The lack of congruency between the historical and geological records is an issue that has been discussed in other paleotempestology studies (Park, 2012; Hippensteel et al., 2013; van Hengstum et al., 2014) and continues to be of interest to the field of Paleotempestology.

In addition, we found that some "intense hurricanes" were still missing from our geologic record, for example Hurricanes Wilma, Charley, Andrew and the Cuba and Labor Day Hurricanes. Several factors may contribute to the lack of paleotempestite deposition in the Angliers Pond including geomorphology of the site (general susceptibility to overwash) and storm dynamics. Geomorphology includes factors such as dune height, distance from the foreshore, and site orientation relative to the coast. Dune height must be considered in concert with storm surge when anticipating paleotempestite deposition. Since historic dune heights are largely unknown, only estimates can be assumed. Nonetheless, coastal regions do exhibit consistent patterns in dune height (Fig. 3B and C). The mean dune height of a region could serve as a storm's minimal surge threshold for potential overwash. In our case, overwash is only likely to occur with a combination of storm surge and waves greater than 1.7 m, which is the modern dune height (beach profile taken 2016). As discussed above, the LiDAR data-generated beach profiles (Fig. 3B and C) show a relatively consistent dune height through time. Therefore, we may not expect to see evidence of Hurricanes Wilma, Charley and Andrew, all of which had known surges of less than 4.5 ft. Unfortunately, due to the lack of tidal gauges it is difficult to test this theory for storms older that 1965. But it does seem apparent that the Angliers Pond is most sensitive to intense, large radius hurricanes that produced significant storm surge.

5.5. Historic hurricane effects on Sanibel Island geomorphology

Due to the lack of overwash deposits in Angliers Pond between 1961 to present day we can assume that storms occurring during this time period have not overwashed the foredune. This is also in line with the relatively low storm surge estimates from these recent storms (Table 1). Recent beach profile data between 1998 and 2015 (Fig. 3A, B and C) indicate that the dune crest and highest section of the beach seaward of Angliers Pond (R-155 and R-156) has been relatively stable through time, though the width of the dune crest itself has varied through time at some locations. At this site the geomorphology of the foreshore varies significantly through time and appears to have been greatly affected by hurricanes. The height of the foreshore is lowest in 1998, and also post-Charley and -Ivan in 2004. By 2010 and 2015 the foreshore had gained in elevation (Fig. 3A, B and C). Savarese et al., (2019) find similar trends on Sanibel Island, where Gulf-side beaches running the length of Sanibel and Captiva Islands are highly dynamic, yet highly stable over the long term. Here they also find that the foredune has been resilient and remained largely undamaged by storm or tidal erosion, or that the dune has naturally repaired itself. Since the above storms had relatively low storm surges it is likely that they reached the "swash" or "collision" regimes (Sallenger, 2000). Under these regimes storm surge does not make it over the foredune, though erosional effects on the foreshore and foredune will be apparent. During these regimes sand can be removed from the foreshore and dune and transported offshore, not always returning to the beach post-storm (Sallenger, 2000).

Unfortunately, historic beach profile data is not available beyond 1998 so it is difficult to assess the effects of older storms such Hurricane Donna (1960), The Great Miami Hurricane (1926) and the Tampa Bay Hurricane (1921). However, due to the presence of overwash sediments in Angliers Pond (tempestites) we believe that these storms reached either the "overwash" or "inundation" regime. During both of these regimes sand from both the beach and the dune is eroded and deposited landward. The "inundation" regime is more intense than the "overwash" regime and in this case a breach of the dune can occur, sometimes causing a new channel to cut through the barrier (Sallenger, 2000). The presence of overwash sediments in Angliers Pond would indicate that these storms had significant erosional effects on the foreshore and dune seaward of the pond. Historic satellite imagery for 1944, 1953, 1958, and 1995 show Angliers pond similar to today, with no tidal to the Gulf of Mexico (Appendix 1E). If any of these storms caused a cut through channel it is not evident in the 1944, 1953, 1958, and 1985 historic images. Unfortunately, post hurricane imagery is unavailable for these storms so it difficult to discern their direct effects on geomorphology.

Coastal exposure to storm surge can lead to significant damage and even loss of life during hurricanes. When storm surge height exceeds the beach crest, an overwash event can occur resulting in the movement of sediment and water across the backside of the beach (Coogan et al., 2019). Today, the population of Sanibel Island is significantly higher than that of the early to mid 1900's, therefore it is important to understand the types of hurricanes in the past that have breached the dune crest. This research indicates that at least three storms made significant impact on Sanibel Island between ~1920–1960. These storms were intense, large radius storms with significant storm surge. Since 1960 no hurricanes have breached the Sanibel Island barrier.

6. Conclusion

Based on the proxy tests and dating of the core samples taken from the Angliers Pond, a modern-day record of intense hurricane strikes dating back to approximately *ca.* 1920 was constructed. Radiometric dating and stratigraphic analyses indicate that the current pond system formed in the mid to late 19th century (*ca.* 1850–1900), and that

previous to this time period the geomorphology of the pond was different, mostly likely a foredune swale. The pond location shifted from a more marine to a more terrestrial environment marked by a distinct facies change in all core samples. Several physical and chemical proxies including grain size, organics (LOI), moisture content, and calcium carbonate, have been used successfully to identify tempestites in the Angliers Pond site. Five of the cores extracted from the pond showed two-three prominent paleo-tempestites (T1-T3). To obtain ages of these events, three cores (1301–39, 1410–51 and 1305–50) were dated using ^{210}Pb. Using the average dates, T1 was constrained between *ca.* 1956 ± 8 and *ca.* 1967 ± 4YR and has been identified as Hurricane Donna (1960). Hurricane Donna overwash consists predominantly of fine-grained sand in the majority of Sanibel cores, with some samples containing higher percentages of shell hash (marine gastropod, marine surf, and others), resulting in a higher calcium carbonate content. Using the average dates, T2 was constrained between *ca.* 1935 ± 21 YR and *ca.* 1950 ± 10 YR. This tempestite consists of both fine-grained sand and coarse broken shell material. Using core 39, T3 was constrained between *ca.* 1935 ± 21 YR and *ca.* 1950 ± 10 YR. It is likely that T2 and T3 were produced by the 1926 Great Miami Hurricane and the Tampa Bay hurricane of 1921.

Declaration of competing interest

The authors declare that they have no known competing financial interests or personal relationships that could have appeared to influence the work reported in this paper.

Acknowledgements

This work was supported by the National Science Foundation (grant numbers 1919813 and 1335375). We would like to thank Dr. Puspa Adhikari for assistance with radiometric dating, Dr. Mike Savarese for assistance with site characterization and Dr. Dhruvkumar Bhatt for assistance with DEM maps.

Appendix A. Supplementary data

Supplementary data to this article can be found online at https://doi.org/10.1016/j.geomorph.2022.108148.

References

Adhikari, P.L., Maiti, K., Overton, E.B., Rosenheim, B.E., Marx, B.D., 2016. Distributions and accumulation rates of polycyclic aromatic hydrocarbons in the northern Gulf of Mexico sediments. Environ. Pollut. 212, 413–423.
Appleby, P.G., Oldfield, F., 1978. The calculation of lead-210 dates assuming a constant rate of supply of unsupported 210Pb to the sediment. Catena 5 (1), 1–8.
Appleby, P.G., Oldfield, F., 1992. Applications of lead-210 to sedimentation studies. In: Uranium-series Disequilibrium: Applications to Earth, Marine, and Environmental Sciences, 2. ed.
Balfour, 1992. Hurricane Andrew Preliminary Report. August 26. National Weather Service Ruskin, Florida. National Hurricane Center. Retrieved December 28, 2011.
Barnes, J., 2007. Florida's Hurricane History. The University of North Carolina Press, North Carolina.
Binford, M.W., 1990. Calculation and uncertainty analysis of 210 Pb dates for PIRLA project lake sediment cores. J. Paleolimnol. 3 (3), 253–267.
Blake, Rappaport, Landsea, 2006. The Deadliest, Costliest, and Most Intense United States Tropical Cyclones (1851 to 2006). NOAA.
Brandon, C.M., Woodruff, J.D., Lane, D.P., Donnelly, J.P., 2013. Tropical cyclone wind speed constraints from resultant storm surge deposition: a 2500 year reconstruction of hurricane activity from St. Marks, FL. Geochem. Geophys. Geosyst. 14 (8), 2993–3008.
Cerrito, E., Mock, C., Collins, J.M., 2021. The Great Havana Hurricane of 1846: a reconstruction of the storm's track, intensity, and impacts. Ann. Assoc. Am. Geogr. https://doi.org/10.1080/24694452.2020.1838257.
Coastal Breeze News Staff, 2010a. 1873 & 1910 hurricanes. June 2010. Coastal Breeze News. Accessed on Aug. 27, 2021. https://www.coastalbreezenews.com/articles/1873-1910-hurricanes/.
Coastal Breeze News Staff, 2010b. 1935 & 1940s hurricanes. July 2010. Coastal Breeze News. Accessed on Aug. 27, 2021. https://www.coastalbreezenews.com/opinion/columnists/1935-1940s-hurricanes/article_edd8c2bc-a16c-57fb-b376-d910af6e2ad0.html.
Collins, J.M., Rohli, R., Paxton, C., 2017. In: Florida Weather and Climate: More than Just Sunshine. University Press of Florida, p. 247.
Coogan, J.S., Webb, B.M., Smallegan, S.M., Puleo, J.A., 2019. Geomorphic changes measured on Dauphin Island, AL, during Hurricane Nate. Shore Beach 87 (4), 15.
Dean, W.E., 1974. Determination of carbonate and organic matter in calcareous sediments and sedimentary rocks by loss on ignition; comparison with other methods. J. Sediment. Res. 44 (1), 242–248.
Dietz, M.E., Bianchette, T.A., Smith, D., Liu, K.-B., 2021. Differentiating hurricane deposits in coastal sedimentary records: two storms, one layer, but different processes. Environ. Res. Commun. 3, 101001.
Donnelly, J.P., Bryant, S.S., Butler, J., Dowling, J., Fan, L., Hausmann, N., Webb III, T., 2001. 700 yr sedimentary record of intense hurricane landfalls in southern New England. Geol. Soc. Am. Bull. 113 (6), 714–727.
Donnelly, J.P., Woodruff, J.D., 2007. Intense hurricane activity over the past 5,000 years controlled by El Nino and the West african monsoon. Nature 447, 465–468.
Doyle, Larry J., Sharma, Dinesh C., Hine, Albert C., Orrin, H., Neal, William J., Orrin, H., Martin, David, Belknap, Daniel F., Jr, Pilkey, Sr, Pilkey, 1984. Living With the West Florida Shore. Duke University Press. ISBN 978-0822305170.
Dunn, G.E., 1961. The hurricane season of 1960. Mon. Weather Rev. 89 (3), 99–108.
Edic, Robert F., 1996. Fisherfolk of Charlotte Harbor, Florida. Institute of Archaeology and Paleoenvironmental Studies, Gainesville, Florida. ISBN 978-1881448044.
Ellis, M., 1984. North Florida and the Great storm of 1873. Retrieved from Fla. Hist. Q. 62 (4), 485–496. http://www.jstor.org/stable/30146596.
Emanuel, K., 2005. Increasing destructiveness of tropical cyclones over the past 30 years. Nature 436, 686–688. https://doi.org/10.1038/nature03906.
Ercolani, C., Muller, J., Collins, J., Savarese, M., Squiccimara, L., 2015. Intense Southwest Florida hurricane landfalls over the past 1000 years. Quat. Sci. Rev. 126, 17–25.
Fernández-Partagás, J.J., Diaz, H.F., 1995. A Reconstruction of Historical Tropical Cyclone Frequency in the Atlantic From Documentary and Other Historical Sources. Climate Diagnostics Center, Environmental Research Laboratories, NOAA.
Fort Myers News-Press Staff, 1944a. October 20, 1944. In: Red Coconut, 15 Cottages Wiped Away, 339. Fort Myers News-Press, Fort Myers, Florida, p. 1, 4.
Fort Myers News-Press Staff, 1944b. October 20, 1944. In: City Escapes Serious Loss in Hurricane, 339. Fort Myers News-Press, Fort Myers, Florida, p. 1, 3.
Hawkes, A.D., Horton, B.P., 2012. Sedimentary record of storm deposits from Hurricane Ike, Galveston and San Luis Islands, Texas. Geomorphology 171–172, 180–189. https://doi.org/10.1016/j.geomorph.2012.05.017.
Heiri, O., Lotter, A.F., Lemcke, G., 2001. Loss on ignition as a method for estimating organic and carbonate content in sediments: reproducibility and comparability of results. J. Paleolimnol. 25 (1), 101–110.
Hippensteel, S.P., Martin, R.E., 1999. Foraminifera as an indicator of overwash deposits, barrier island sediment supply, and barrier island evolution, Folly Island, South Carolina. Palaeogeogr. Palaeoclimatol. Palaeoecol. 149, 115–125.
Hippensteel, S.P., 2011. Spatio-lateral continuity of hurricane deposits in back-barrier marshes. Bulletin 123 (11–12), 2277–2294.
Hippensteel, S.P., Eastin, M.D., Garcia, W.J., 2013. The geological legacy of Hurricane Irene: implications for the fidelity of the paleo-storm record. GSA Today 23 (12), 4–10.
Landsea, C.W., Hagen, A., Bredemeyer, W., Carrasco, C., Glenn, D.A., Santiago, A., Strahan-Sakoskie, D., Dickinson, M., 2013. A reanalysis of the 1931–43 Atlantic Hurricane database. J. Climatol. 27, 6093–6118.
Landsea, C.W., Anderson, C., Charles, N., Clark, G., Dunion, J., Fernandez-Partagas, J., Hungerford, P., Neumann, C., Zimmer, M., 2004. In: Murnane, R.J., Liu, K.B. (Eds.), The Atlantic Hurricane Database Reanalysis Project—Documentation for 1851–1910 Alterations and Additions to the HURDAT Database. Hurricanes and Typhoons: Past, Present, and Future. Columbia University Press in press.
Leorri, E., Cearreta, A., Irabien, M.J., Garcia-Artola, A., Corbett, D.R., Horsman, E., Blake, W.H., Sanchez-Cabeza, J.A., 2014. Anthropogenic disruptions of the sedimentary record in coastal marshes: examples from the southern Bay of Biscay (N. Spain). Cont. Shelf Res. 86, 132–140.
Li, Z., Weisberg, R.H., 1999. West Florida shelf response to upwelling favorable wind forcing: Kinematics. J. Geophys. Res. Oceans 104 (C6), 13507–13527.
Liu, K.B., Fearn, M.L., 1993. Lake-sediment record of late Holocene hurricane activities from coastal Alabama. Geology 21, 793–796.
Liu, K.B., Fearn, M.L., 2000. Reconstruction of prehistoric landfall frequencies of catastrophic hurricanes in northwestern Florida from lake sediment records. Quat. Res. 54 (2), 238–245.
Marston, R., 1960. Disaster, Thy Name Was Donna and For Many Stark Despair. St. Petersburg Times. September 22, 1960. 1B and 17B.
McDonald, W.F., 1935. The hurricane of August 31 to September 6, 1935. Mon. Weather Rev. 63, 269–271.
Missimer, T.M., 1973. Growth rates of beach ridges on Sanibel Island, Florida. In: Gulf Coast Association of Geological Societies Transactions, 22, pp. 383–388.
Myrow, P.M., Southard, J.B., 1996. Tempestite deposition. J. Sediment. Res. 66, 875–887.
NOAA's National Hurricane Center, 1960. Tropical cyclones reports, Hurricane Donna, September, 1960. www.nhc.noaa.gov.
NOAA, 2004. Hurricane Charley preliminary water levels report. September 2004. https://tidesandcurrents.noaa.gov/publications/HurricaneCharley2004PreliminaryWaterLevelsReport.pdf.
NOAA, 2020. Record -breaking Atlantic hurricane season draws to an end. https://www.noaa.gov/media-release/record-breaking-atlantic-hurricane-season-draws-to-end. Acessed 25 Sept. 2021.

NOAA National Centers for Environmental Information, 2021. U.S. billion-dollar weather and climate disasters. https://www.ncdc.noaa.gov/billions/. ISBN 978-0822305170.

Oertel, G.F., 2005. Coastal lakes and lagoons. In: Schwartz, M.L. (Ed.), Encyclopedia of Coastal Science, Encyclopedia of Earth Science Series. Springer, Dordrecht. https://doi.org/10.1007/1-4020-3880-1_81.

Otvos, E., 2000. Beach ridges — definitions and significance. Geomorphology 32, 83–108.

Park, L.E., 2012. Comparing two long-term hurricane frequency and intensity records from San Salvador Island, Bahamas. J. Coast. Res. 28 (4), 891–902.

Parsons, M.L., 1998. Salt marsh sedimentary record of the landfall of Hurricane Andrew on the Louisiana coast: diatoms and other paleoindicators. J. Coast. Res. 939–950.

Pielke Jr., R.A., Landsea, C.W., 1998. Normalized Atlantic hurricane damage, 1925–1995. Weather Forecast. 13, 621–631.

Pine Island Eagle Staff, 2013. This month in history: we may not be out of the woods. Available online:. Pine Island Eagle. Accessed on Aug. 28, 2021. http://pineisland.info/index/hurricane-history/.

Rappaport, E.N., Fernández-Partagás, J.J., 1996. The Deadliest Atlantic Tropical Cyclones, 1492 – 1996: Cyclones With 25+ Deaths. National Hurricane Center https://www.nhc.noaa.gov/ pastdeadlyapp1.shtml?

Robbins, J.A., Edgington, D.N., Kemp, A.L.W., 1978. Comparative 210Pb, 137Cs, and pollen geochronologies of sediments from Lakes Ontario and Erie. Quat. Res. 10 (2), 256–278.

Sallenger Jr., A.H., 2000. Storm impact scale for barrier islands. J. Coast. Res. 890–895.

Savarese, M., Walker, K.J., Stingu, S., Marquardt, W.H., Thompson, V.D., 2006. The effects of shellfish harvesting by Aboriginal inhabitants of Southwest Florida (USA) on productivity of the Eastern Oyster: Implications for estuarine management and restoration. Anthropocene 16 (2016), 28–41.

Savarese, M., Jose, F., Gross, A., Arnett, K., Evans, J., Caouette, J., 2019. An assessment of coastal vulnerability due to sea-level rise and increased storminess, Sanibel and Captiva Islands, Florida. June 2010. Florida Gulf Coast University, and City of Sanibel Department of Natural Resources. Accessed on Aug. 27, 2021. https://www.mysanibel.com/content/download/26673/171010/file/Savarese%20etal%202019%20Sanibel%20Community%20Report%20Complete_FINAL_11-18-19.pdf.

State Library and Archives of Florida, 2017. Rescue train swept off the tracks by the 1935 Labor Day Hurricane. In: World Digital Library https://www.wdl.org/en/item/14203/#additional_subjects =Labor+Day+Hurricane%2C+1935). Accessed 28 Aug., 2021.

Singleton, A.A., Schmidt, A.H., Bierman, P.R., Rood, D.H., Neilson, T.B., Greene, E.S., Perdrial, N., 2017. Effects of grain size, mineralogy, and acid-extractable grain coatings on the distribution of the fallout radionuclides 7Be, 10Be, 137Cs, and 210Pb in river sediment. Geochim. Cosmochim. Acta 197, 71–86.

Sugg, A.L., Pardue, L., Carrodus, R.L., 1971. Memorable hurricanes of the United States since 1873.

The Vicksburg Herald, 1921. Fort Myers, Florida. October 27. In: Fort Myers Hit Hard, p. 3. Archived from the original on April 6, 2017. Retrieved April 5, 2017 – via Newspapers.com. open access.

U.S. Army Corps of Engineers, Jacksonville District., 1969. Beach erosion control study on Lee County, Florida: Jacksonville. Florida. Series No. 60, 41.

US Department of Commerce, 1960. In: Climatological Data, Florida. September 1960, 64(9), p. 36.

van Hengstum, P.J., Donnelly, J.P., Toomey, M.R., Albury, N.A., Lane, P., Kakuk, B., 2014. Heightened hurricane activity on the Little Bahama Bank from 1350 to 1650 AD. Cont. Shelf Res. 86, 103e115.

Wang, R., Manausa, M., Cheng, J., 2005. Hurricane Charley characteristics and storm tide evaluation. In: Beaches and Shores Resource Center, Institute of Science and Public Affairs, Florida State University, Tallahassee, FL, USA. ISBN 978-0822305170.

Weinkle, J., Landsea, C., Collins, D., Musulin, R., Crompton, R.P., Klotzbach, P.J., Pielke, R., 2018. Normalized hurricane damage in the continental United States 1900–2017. Nat. Sustain. 1 (12), 808.

Williams, H.F.L., Denlinger, E., 2013. Contribution of Hurricane Ike storm surge sedimentation to long-term aggradation of Southeastern Texas coastal marshes. J. Coast. Res. 65 (1), 838–843. https://doi.org/10.2112/SI65-142.1.

Williams, H.F.L., Liu, K.-B., 2021. Testing XRF discrimination of marine and terrestrial flood deposits in southeastern Texas coastal marshes. J. Coast. Res. 37 (6), 1081–1087.